Figure 1.

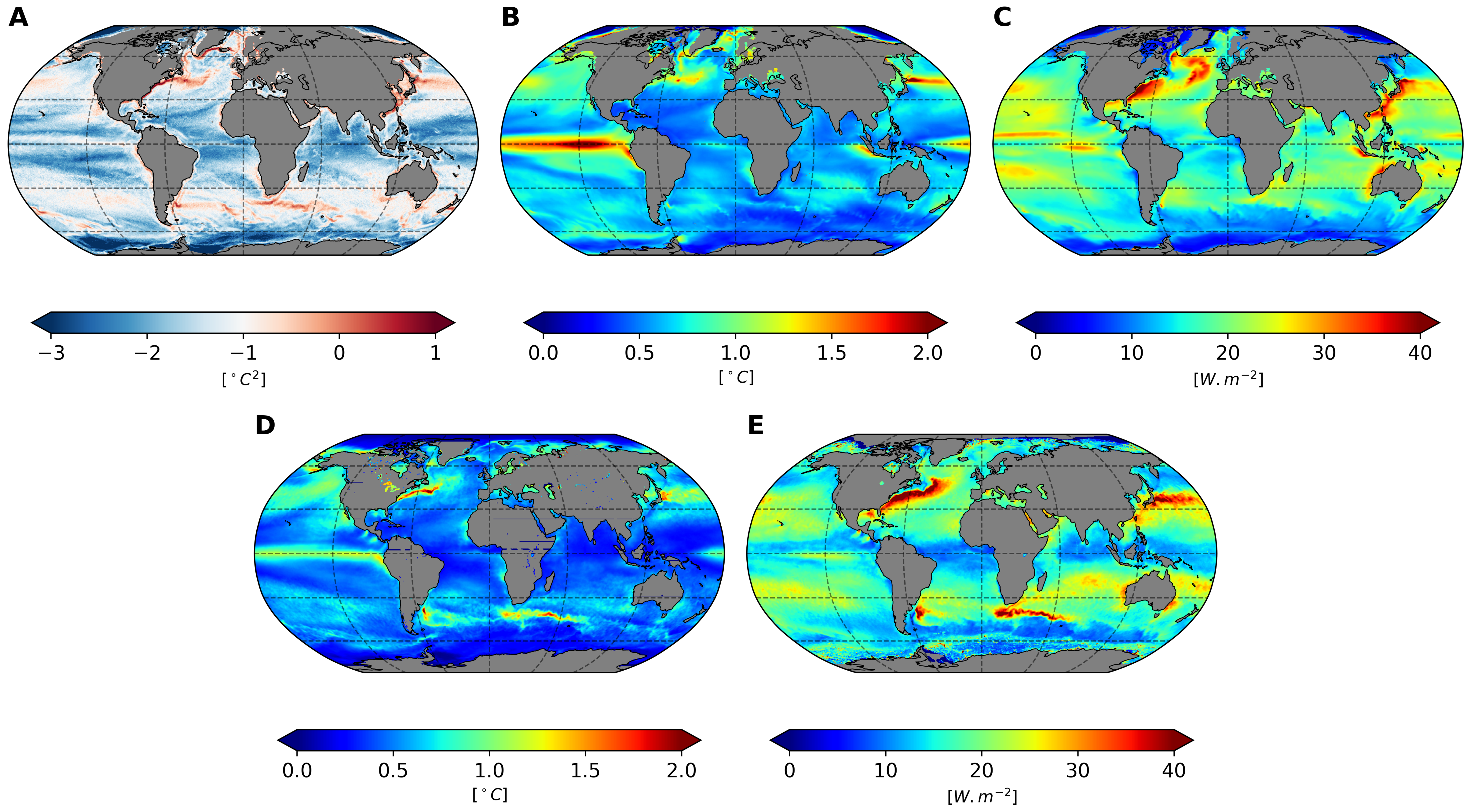
A
B
C
−3
−2
−1
0
1
[$^\circ C^2$]
0.0
0.5
1.0
1.5
2.0
[$^\circ C$]
0
10
20
30
40
[$W.m^{-2}$]
D
E
0.0
0.5
1.0
1.5
2.0
[$^\circ C$]
0
10
20
30
40
[$W.m^{-2}$]

Figure 2.

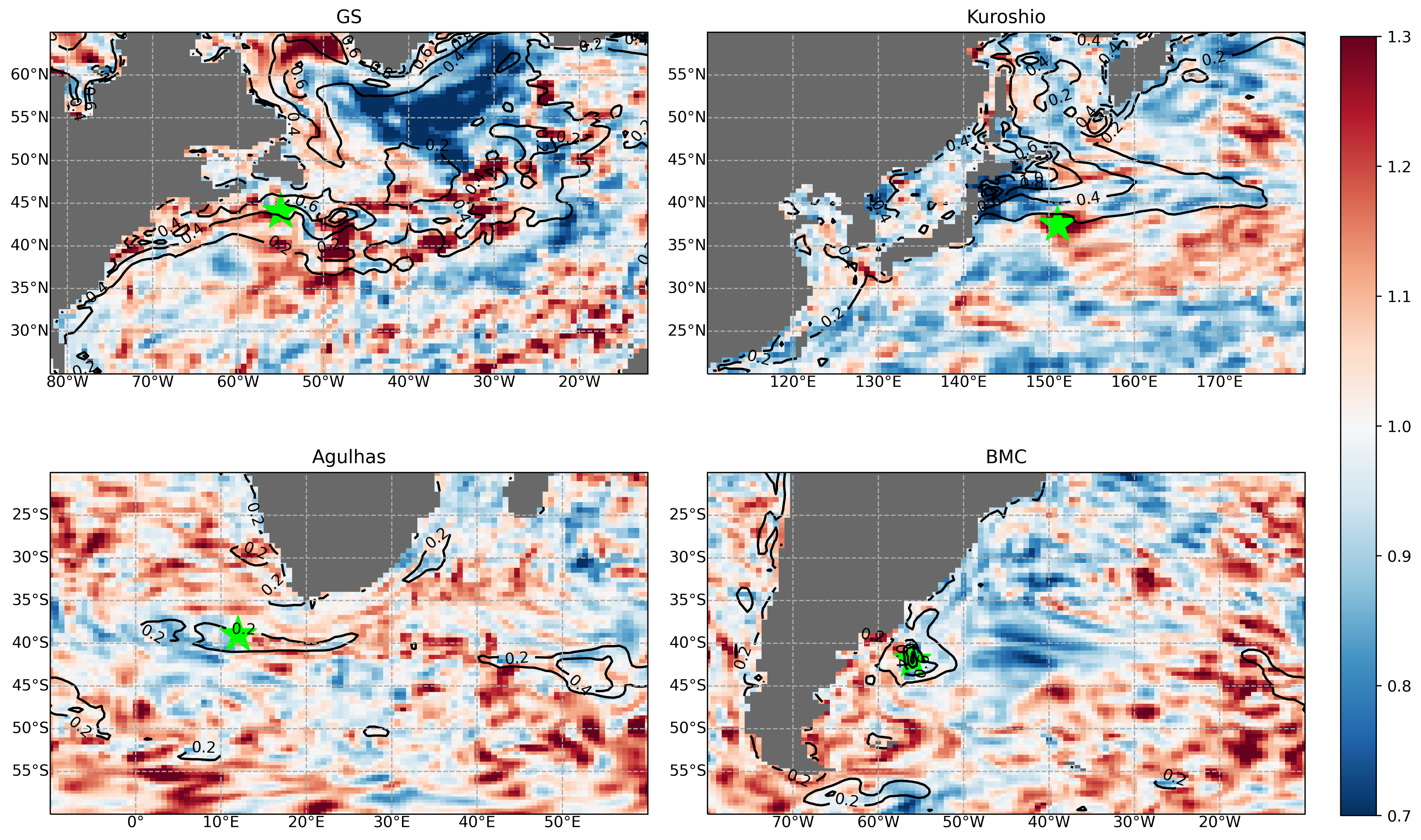

GS
Kuroshio
Agulhas
BMC
60°N
55°N
50°N
45°N
40°N
35°N
30°N
25°N
80°W
70°W
60°W
50°W
40°W
30°W
20°W
120°E
130°E
140°E
150°E
160°E
170°E
25°S
30°S
35°S
40°S
45°S
50°S
55°S
0°
10°E
20°E
30°E
40°E
50°E
0.2
0.4
0.6
0.8
0.7
0.9
1.0
1.1
1.2
1.3

Figure 3.

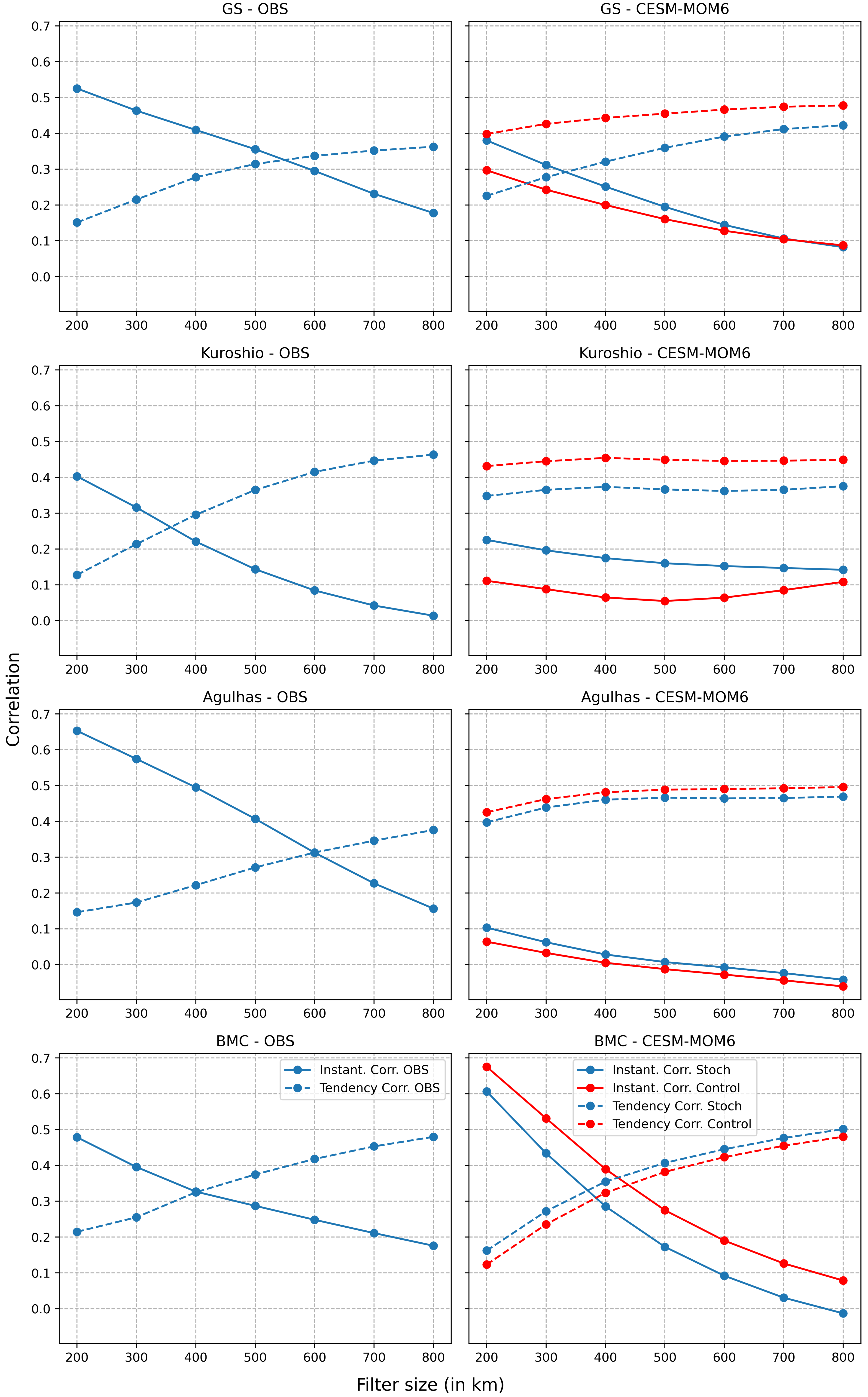

GS - OBS
GS - CESM-MOM6
Kuroshio - OBS
Kuroshio - CESM-MOM6
Agulhas - OBS
Agulhas - CESM-MOM6
BMC - OBS
BMC - CESM-MOM6
Instant. Corr. OBS
Tendency Corr. OBS
Instant. Corr. Stoch
Instant. Corr. Control
Tendency Corr. Stoch
Tendency Corr. Control
Correlation
Filter size (in km)

Impact of stochastic ocean density corrections on air-sea flux variability

Niraj Agarwal[1], R. Justin Small[3], Frank O. Bryan[3], Ian Grooms[2], Philip J.Pegion[4]

[1]University of Colorado Boulder/CIRES, Boulder, CO, USA
[2]Department of Applied Mathematics, University of Colorado Boulder, Boulder, CO, USA
[3]Climate and Global Dynamics Laboratory, National Center for Atmospheric Research, Boulder, CO, USA
[4]NOAA Physics Sciences Division, Boulder, CO, USA

Key Points:

- A subgrid-scale parameterization for ocean density is applied to improve the ocean-intrinsic air-sea flux variability in a climate model.
- The parameterization modifies the SST and latent heat flux variability at the ocean grid-scale level and boosts their local correlations.
- The stochastic parameterization improves consistency with observations.

Corresponding author: Niraj Agarwal, `niraj.agarwal@colorado.edu`

Abstract

Air-sea flux variability has contributions from both ocean and atmosphere at different spatio-temporal scales. Atmospheric synoptic scales and the air-sea turbulent heat flux that they drive are well represented in climate models, but ocean mesoscales and their associated variability are often not well resolved due to non-eddy-resolving spatial resolutions of current climate models. We deploy a physics-based stochastic subgrid-scale parameterization for ocean density, that reinforces the lateral density variations due to oceanic eddies, and examine its effect on air-sea heat flux variability in a comprehensive coupled climate model. The stochastic parameterization substantially modifies sea surface temperature (SST) and latent heat flux (LHF) variability and their correlations, primarily at scales near the resolution of the ocean model grid. Changes in the SST-LHF anomaly correlations indicate that the ocean-intrinsic component of the air-sea heat flux variability improves with respect to the satellite observational product, especially in western boundary current extensions.

Plain Language Summary

Variations in air-sea heat fluxes arise from both ocean and atmosphere at different space and time scales. Studies suggest that at large scales, e.g., thousands of kilometers, atmospheric processes drive the ocean variability at the surface, such as sea-surface temperature. However, at smaller spatial scales, e.g., $[100-1000]$ km, the oceans control the atmosphere variability near the air-sea interface. These local air-sea feedbacks influence both oceans and the atmosphere on various levels and are of significant dynamical importance. However, climate models typically use large grid spacing and fail to represent the air-sea interaction mechanism inherent to these small scales. We address this problem by modifying the ocean density using random noise at multiple places in the model before coupling it to the atmosphere. We chose density because it is used for multiple purposes in ocean models, and imperfections in it arise due to the missing subgrid-scale effects that can have a major impact all over the oceans, especially the upper ocean which interacts the most with the atmosphere. The proposed approach led to significant improvement in the air-sea interaction properties at various spatial scales compared to satellite observations.

1 Introduction

Air-sea coupling plays a key role in shaping the Earth's climate and representing it correctly is essential for reducing the uncertainties in climate projections. Theoretical studies and satellite observations suggest that the mechanisms that control this coupling are largely length- and time-scale-dependent. In mid-latitudes and extratropics, synoptic-scale atmospheric weather patterns drive turbulent heat flux (THF) variability at scales larger than or equal to $\mathcal{O}(10^3)$ km through wind speed fluctuations and air-sea temperature and humidity anomalies. The generated THF anomaly receives a lagged response from the oceans, for example; heat loss from the oceans leading to cooling of the oceans on a timescale of several weeks (Xie, 2004). In contrast, at mesoscales (10^1-10^3 km), persistent and vigorous intrinsic eddy variability in the oceans creates strong SST anomalies and as the wind passes over them, strong air-sea temperature and humidity differences are generated that drive the THF variability (Hausmann et al., 2017). This mechanism is well represented in idealized coupled model studies, such as Hasselmann (1976); Frankignoul and Hasselmann (1977); von Storch (2000), where the atmospheric and oceanic forcings are specified stochastically, and their dominance is tuned using the noise amplitude.

However, most global climate models employ ocean models at a non-eddy-resolving resolution, or eddy-permitting resolution at best, and therefore do not resolve the ocean mesoscale eddies (10-100 km) and the respective impact on the air-sea flux variability.

This is clearly problematic because studies have shown that the relative contributions of intrinsic oceanic and atmospheric variability in air-sea flux modulation bear enormous dynamical implications both for the oceans (Ma et al., 2016) and the atmosphere (Kuo et al., 1991; Minobe et al., 2008; Ma et al., 2017; Williams, 2012). The reader is referred to Czaja et al. (2019) for a concise review of the state of knowledge of modeled atmosphere response to mid-latitude SST and their scale dependence. The midlatitude SST fluctuations on scales close to the ocean deformation scale (i.e., 10-100 km) significantly affect the variability of lower atmosphere (reviewed in Small et al. (2008)) and the predictability of the midlatitude weather system (Dunstone et al., 2016). Contemporary studies involving ultra high-resolution of the atmosphere are starting to divulge the physical mechanisms by which such small-scale oceanic variability is communicated to the troposphere above the atmospheric boundary layer (Parfitt et al., 2016; Foussard et al., 2019). These results underscore the importance of parameterizing/resolving such eddy variability at the ocean gridscale in order to reduce the uncertainty in air-sea fluxes and their climatic impacts.

In this work, we employ a stochastic subgrid-scale (SGS) parameterization for ocean density and study its impact on air-sea THF variability in a coupled climate model. Ocean density depends on temperature T, salinity S, and pressure p through a nonlinear equation of state (EOS); SGS fluctuations in T and S cause the grid-cell-averaged density to be different from that obtained by evaluating the EOS at the grid-cell-averaged values of T and S (pressure fluctuations are sub-dominant). Brankart (2013) first proposed a parameterization for these density errors and discussed their non-trivial global impacts. An alternative parameterization, which is more accurate and more computationally efficient, was proposed by Stanley et al. (2020) and tested in an ocean-only configuration by Kenigson et al. (2022). Whereas Kenigson et al. (2022) only tested the parameterization in the computation of the buoyancy force and associated hydrostatic pressure, we use this parameterization to correct density at three places in the ocean model: the hydrostatic pressure, isopycnal slopes in the Gent-McWilliams parameterization (hereinafter, GM; Gent and McWilliams (1990)), and the mixed-layer lateral buoyancy gradient in the mixed-layer restratification parameterization of Fox-Kemper et al. (2008). In this study, we aim to explore the possibility of employing this stochastic parameterization of the mesoscale eddy effects on density to strengthen the ocean-intrinsic SST variability and its impact on air-sea THF variability.

2 Theory and Methods

2.1 SGS Density Parameterization

The ocean density correction used in this paper derives from the Taylor expansion of the nonlinear EOS (denoted as $\hat{\rho}$) about the grid-cell average quantities. Following the notations used in Stanley et al. (2020), the corrected grid-cell-mean density (denoted $\overline{\rho}$) is given as,

$$\overline{\rho} = \hat{\rho}(\overline{T}, \overline{S}, \overline{p}) + \frac{\partial_T^2 \hat{\rho}(\overline{T}, \overline{S}, \overline{p})}{2} \sigma_T^2, \tag{1}$$

where $\overline{T}(x, y, z, t)$ and $\overline{S}(x, y, z, t)$ are grid-cell-averaged temperature and salinity, respectively, and $\sigma_T^2(x, y, z)$ is the variance of unresolved SGS temperature. The stochastic parameterization proposed by Stanley et al. (2020) for σ_T^2 is

$$\sigma_T^2 = c e^{\chi} |\delta x \circ \nabla \overline{T}|^2. \tag{2}$$

Here $\nabla \overline{T}$ is the lateral gradient of the resolved temperature field, δx is the horizontal grid size, $\circ$ is the Hadamard product, $\chi(x, y, t)$ is a depth-independent normally-distributed random noise with zero mean and variance σ_χ^2, and c is a tunable parameter. Stanley et al. (2020) performed a rigorous offline diagnostic for the parameter c for different spatial resolutions of the target model and suggested $c = 0.25$ for our model resolution.

However, following Kenigson et al. (2022) we increase this value to $c = 0.5$ to account for the weaker resolved temperature gradients in a coarse-model simulation compared to those obtained by coarsening a high-resolution simulation. The log-normal form of noise is chosen based on the statistical analysis of the residuals from the deterministic form (i.e., Eq. 2 without the term e^{χ}), and the multiplicative formulation is adopted to ensure the parameterization expression is always positive, as we are approximating variance. Furthermore, χ is uncorrelated in space but has the following AR(1) structure in time

$$\chi(x, y, t) = \phi(x, y, t)\chi(x, y, t - \delta t) + \epsilon(x, y, t), \tag{3}$$

where $\epsilon(x, y, t)$ is a zero-mean Gaussian random noise with no correlations in space and time. The variance of ϵ varies with the AR(1) parameter $\phi(x, y, t)$ such that the process variance σ^2_χ remains constant; Stanley et al. (2020) found $\sigma^2_\chi = 0.39$. Next, $\phi(x, y, t)$ is expressed using the decorrelation time scale (τ) of the local kinetic energy as

$$\phi(x, y, t) = e^{\frac{\delta t}{\tau(x,y,t)}}, \tag{4}$$

where δt is the model baroclinic time step and τ is equal to

$$\tau(x, y, t) = k\sqrt{\frac{\delta x^2 + \delta y^2}{u^2 + v^2}}. \tag{5}$$

Here $u(x, y, t)$ and $v(x, y, t)$ are the upper-ocean instantaneous velocities, and $k = 3.7$ is a tunable parameter whose value was estimated by Stanley et al. (2020). The decorrelation timescale τ essentially depends on the resolved fields, and the offline diagnostics have shown that it varies between a few days to several months for 2/3° resolution ocean model. The global map of the parameterized SGS temperature variance for a 2/3° resolution MOM6 simulations stored as monthly mean is shown in Figure 1a. It is easy to note that the variance is significantly higher in mid-latitude western boundary current (WBC) regions compared to the tropics (note the logarithmic scaling). This is due to the enormous lateral temperature gradients and strong mesoscale eddy variability present in those regions.

2.2 Model and Observations

We tested the above parameterization in the Modular Ocean Model, version 6, (MOM6) ocean general circulation model which solves the hydrostatic primitive equations on a tripolar grid with C-grid horizontal stencil. It uses an Arbitrary Lagrangian-Eulerian vertical coordinate method (Adcroft et al., 2019; Griffies et al., 2020) and the energetically consistent mesoscale backscatter proposed byJansen et al. (2019) involving mesoscale eddy kinetic energy budget and GM parameterization. MOM6 is coupled to Los-Almos Sea Ice Model, version 5, (CICE5; Hunke et al. (2010)) in the Community Earth System Modeling Version 2.3, (CESM2) framework. The model uses the GEOMETRIC parameterization (Marshall et al., 2012) to set the GM coefficient κ. Explicit diapycnal mixing in the oceans due to convection and static instabilities is not permitted due to the hydrostatic approximation, but is parameterized using the K-profile parameterization (KPP) proposed in Large et al. (1994); restratification of the mixed layer is handled using the FFH parameterization (Fox-Kemper et al., 2008). The Wright EOS (Wright, 1997) is used to compute density as a function of pressure, temperature, and salinity.

We configured CESM-MOM6 as a fully coupled global ocean-atmosphere-sea ice model with 2/3° nominal spatial resolution for the ocean and sea-ice model and a coarser 0.95°×1.25° resolution for the atmosphere and the land component. The ocean model uses 65 vertical levels in z* coordinates (Adcroft & Campin, 2004) with finer vertical resolution around the ocean surface (2.5m) and coarser towards the bottom (≈ 250m) and integrated using a baroclinic time step of 1800 seconds. The atmosphere is represented using the finite-volume based Community Atmospheric Model Version 6 (CAM6; Danabasoglu et al. (2020)) where the atmospheric primitive equations are discretized on 70 vertical

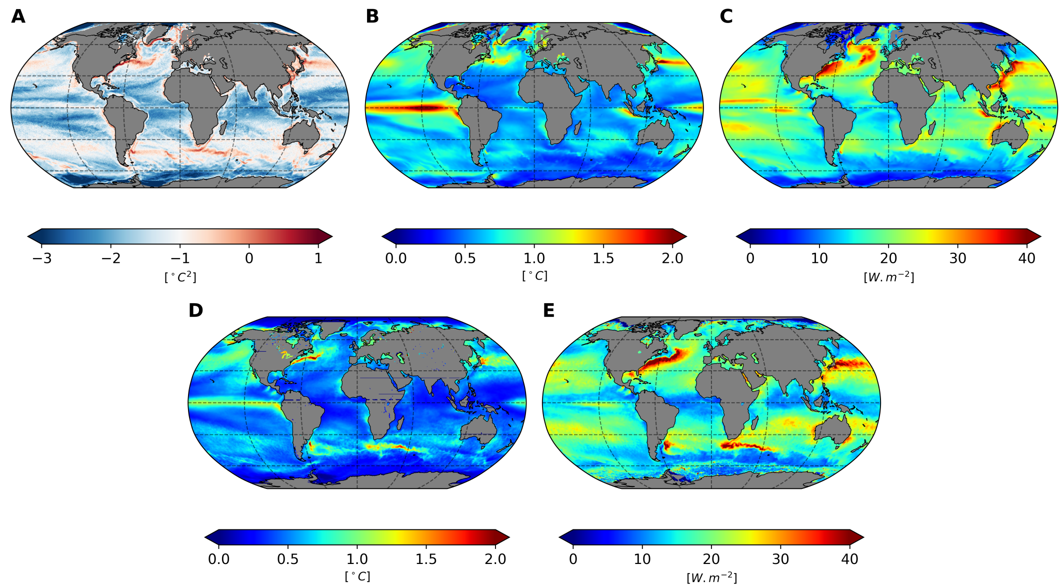

Figure 1. Illustration of the characteristics of the SGS density parameterization, model, and observations: (a) Spatial pattern of the parameterized SGS SST variance using (2); (b)-(c) Standard deviation of monthly anomalies of SST and LHF, respectively, from CESM-MOM6 Stoch simulation; (d)-(e) Same as (b)-(c) but for the J-OFURO3 observations for the period 2000-2015. The monthly anomalies were computed by removing the monthly climatology and the linear trend. In (a), the variance is scaled using log_{10}, and the color bar denotes the exponent of 10.

levels and integrated using a time step of 300 seconds. The atmosphere, sea-ice, and land communicate their fluxes and state information every 30 mins via the CESM coupler bundled with the Earth System Modeling Framework (ESMF) distribution. The air-sea fluxes are computed within the coupler and are passed to the atmospheric model every 30 mins and to the ocean model every hour. The model was run for a total of 100 years under the pre-industrial greenhouse gas conditions with and without the stochastic SGS density parameterization, referred to here as Stoch and Control, respectively. In this study, we have analyzed monthly means from the last 35 years of both experiments. We used monthly-mean products because mesoscale ocean eddy variability is strongest on monthly to annual time scales, and the employed eddy parameterization can be expected to produce notable impacts on these frequencies.

The benchmarking observational products of SST and surface heat fluxes used in this paper are taken from a remote-sensing-based third-generation Japanese ocean flux dataset, abbreviated J-OFURO3 (Tomita et al. (2019); hereinafter, also referred to as OBS). It provides datasets for surface heat, momentum, freshwater fluxes, and the associated physical parameters over the ice-free global oceans from 1986-2017 in daily and monthly-mean temporal resolutions with 0.25 degrees spatial resolution; we used the monthly mean products. J-OFURO project computes the turbulent surface fluxes using a bulk method where all physical parameters are satellite-derived except the 2m air temperature, which is obtained from the NCEP-DOE reanalysis product. The latest version, i.e. J-OFURO3, is a significant advancement over its predecessors as it uses state-of-the-art algorithms to estimate near-surface specific humidity and employs advanced techniques to combine multi-satellite sensor outputs. In addition, rigorous and systematic validations against the in-situ observations and other datasets ensure more accuracy for J-OFURO3.

The OBS version 1.1 monthly-mean products are available from 1988-2017, but we only used the years 2000-2015 in this paper to avoid data gaps.

For a basic illustration of the OBS and model outputs, standard deviations of the monthly anomalies of SST and LHF from the Stoch simulation and OBS are shown in Figure 1(b-e). While the spatial patterns of the SST and LHF variability are similar for both OBS and Stoch, the magnitude of the variability differs across them. This is especially true near the ocean jets and currents, such as Gulf Stream (GS), Kuroshio, Oyashio, Agulhas, and Brazil-Malvinas confluence, which are the areas of focus in this study. These major jets and currents generally show a stronger SST/LHF variability in OBS than in the CESM-MOM6 simulation. Kuroshio is an exception to this, as the Stoch simulation possesses stronger and more eastward extended sub-monthly SST variability in this region (compare Figure 1b and d). This is a known bias related to the convergence of the mean kinetic energy and the largest SST gradient regions (Thompson & Kwon, 2010). Additionally, Stoch possesses significantly high LHF variability around the Labrador and Irminger seas region, which is perhaps related to a known long-term bias in this region. Nevertheless, the generally reduced variance around the jets in model simulations is expected due to their coarse spatial resolution, which does not permit mesoscale eddies and their large-scale feedback and the difference in the lengths of model simulation and OBS products.

2.3 Analysis Methods

In this paper, we consider the latent heat flux (LHF) and SST for all our analyses. We only focus on the LHF component of the net surface heat flux because several previous studies have shown that latent heat dominates the net surface heat flux response to the SST; the contributions from the sensible and radiative heat fluxes are sub-dominant (Frankignoul & Kestenare, 2002; Park et al., 2005; Hausmann et al., 2017). In CESM simulations, LHF is computed using a bulk flux formula – proportional to the air density, wind speed, and difference in the specific humidity saturated at the ocean surface (strongly dependent on SST) and of the air. The invoked parameterization influences LHF through the resolved variables for the oceans and the atmosphere used in the bulk formula.

In this paper, we focus only on local air-sea interactions and study the changes produced therein by the stochastic SGS density parameterization. As discussed in Section 1, at ocean mesoscales, the LHF variability is driven by intrinsic SST variability, led by the mesoscale eddies. We call this SST variability intrinsic because it is not forced by air-sea heat flux anomalies unlike in the case of slow SST variations over large spatial scales. As a result of ocean-driven LHF variability, large outgoing heat flux is noticed over warm SST anomalies, and less heat flux is seen departing over the colder SST anomalies (Small et al., 2008, 2019). This suggests a positive instantaneous correlation between SST and LHF, where the sign convention is that the outgoing heat flux from the oceans is considered positive and incoming is negative. In contrast, at large scales (e.g., ocean basin size), the air is more in equilibrium with the slow-varying SST beneath it and leads to situations where significant outgoing heat flux from the oceans, driven by atmospheric forcing, is seen to cool the oceans. This refers to lagged SST (or, ocean) response to air-sea heat flux variations, i.e., small instantaneous SST-LHF correlation but large $\partial(\mathrm{SST})/\partial t$-LHF correlation (Wu et al., 2006; Bishop et al., 2017; Small et al., 2019). Throughout this paper, we will use the term 'instantaneous correlation' to refer to the simultaneous SST-LHF correlation and 'tendency correlation' to refer to the $\partial(\mathrm{SST})/\partial t$-LHF correlations. We use these two types of correlations to infer the dominant forcing in the ocean-atmosphere feedback mechanism, i.e., (1) if the instantaneous correlation is large, it suggests ocean (precisely, SST) forcing the atmosphere (or, latent heat flux variability), whereas (2) if $\partial(\mathrm{SST})/\partial t$-LHF is large, it means the atmosphere driving the oceans. While (1) is believed to hold true at small scales, (2) is supposed to be the case at large scales. Because the SGS density parameterization corrects the ocean density on ocean mesoscales, it is expected to have a more significant impact on instantaneous correlations than tendency correlations, as synoptic-scale atmospheric processes are already well resolved in climate models. It bears noting that the $2/3°$ ocean model resolution does not resolve the mesoscale, so the direct impact of ocean mesoscales on LHF variability must be absent from the model. But ocean mesoscales induce ocean-intrinsic variability at larger scales that are resolved, a process that is represented in part using the stochastic parameterization.

Because we intend to study the scale dependence of local correlations, we use a spatial filter on the original fields to separate the eddying part from their large-scale counterpart. We use a fast, efficient python package named GCM-Filters (Loose et al., 2022), which achieves filtering using an iterative application of a discrete Laplacian, resembling diffusion (Grooms et al., 2021). We use the Taper filter shape described by Grooms et al. (2021), which makes a sharper separation between large and small scales than Gaussian or boxcar filters. We used filtering length scales from 200 km up to 800 km with a spacing of 100 km. Although the term 'eddy' is frequently used to describe the small-scale part of a field produced by a high-pass spatial filter, we use the term sub-filter scale (SFS) to avoid confusion, since our model does not resolve mesoscale eddies. A monthly climatology (for both SST and LHF) is then computed and subtracted from the monthly-mean values to provide the monthly anomalies, followed by the removal of linear trend.

3 Results

In this section, we diagnose the impact of the SGS stochastic density corrections on the variability and co-variability of SST and LHF and pinpoint the gains/losses by comparing against the J-OFURO3 observational outputs. We also make efforts to explain the identified parameterization impacts from a physical perspective. Furthermore, because the parameterization is mostly active near the regions of strong temperature fronts (see Figure 1a), from here onward we only focus on four regions: the GS and Kuroshio in the northern hemisphere, and the Agulhas and Brazil-Malvinas Confluence (BMC) in the southern hemisphere.

3.1 Sub Filter Scale Variability

To elucidate the modifications produced by the SGS density parameterization across scales, maps of the ratio of the standard deviations of the SFS SST from Stoch and Control runs are shown in Figure 2. Here, the SFS fields are obtained using a filter size of 500 km. It is evident that the density corrections produced by the parameterization significantly affect the SFS SST variability – as much as 30% shift in their standard deviation – in all four regions. While Agulhas is predominantly characterized by a net increase in their SFS variability, GS, Kuroshio, and BMC display a mixed response, i.e., both increase (red) and decrease (blue). An increase/decrease in variability in the form of a red/blue dipole suggests that the parameterization is making dynamical adjustments by changing the positions of the mean currents (cf. Kenigson et al., 2022).

In case of the GS, an increase in SFS variability is clear in the eastward extension portion of the jet between $35°-45°$ N and $30°-60°$W. This is a prominent feature of the parameterization, as several previous idealized studies have shown that mesoscale eddying features are paramount to producing eastward extension of jets (Shevchenko & Berloff, 2015; Agarwal et al., 2021). However, either minimal increase or a decrease in the variability is seen around the far-east extension of the jet. It is also intriguing to spot a region of significantly reduced SFS SST variability in the Irminger Sea and partly in the Labrador Sea between $50°-60°$N and $30°-50$W. This is related to an increase in mixed-layer depth in this region (not shown), which increases the heat capacity of the mixed-layer column and, therefore, a decrease in the variation of the surface tempera-

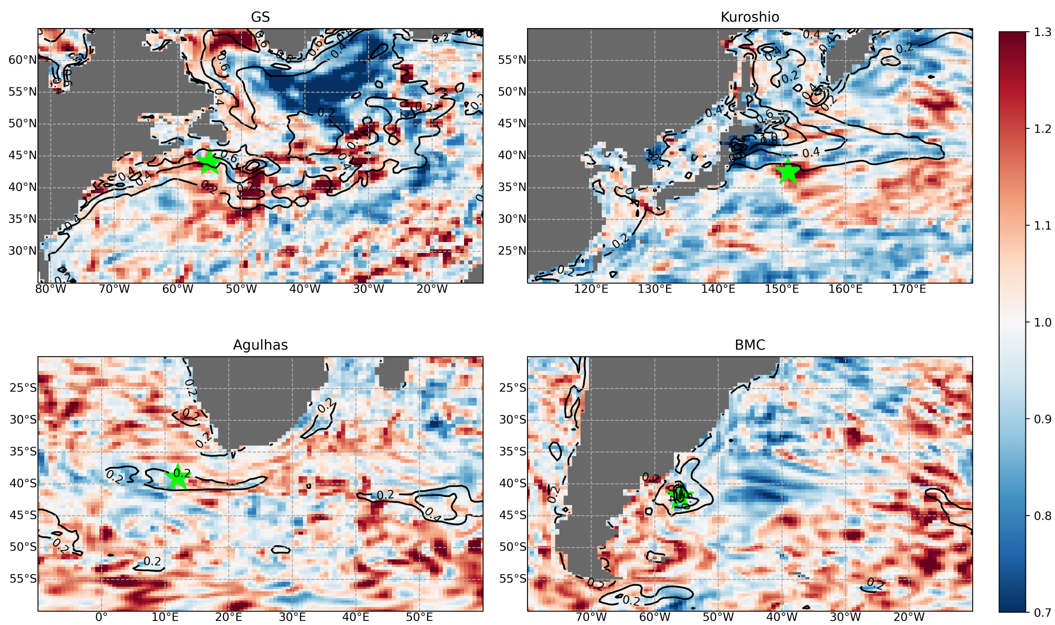

Figure 2. Manifestation of the influence of the stochastic parameterization on variability across different scales. Ratio of the standard deviation of SFS SST from Stoch and Control simulations in four most eminent frontal regions: GS, Kuroshio, Agulhas, and BMC. The filter size used here is 500 km. The ratio is taken as Stoch over Control, so the red/blue indicates an increase/decrease in the SFS SST variability due to the induced parameterization. The contour lines belong to the standard deviations of the SFS SST from the Control experiment. The stars denote the locations picked for the analysis in section 3.2 (in BMC, the star is at 42°S, 56°W). The color scale is in dimensionless units.

ture (more heat is now required to change the surface temperature by $1°C$). The Kuroshio extension mostly witnesses a decrease in the SFS SST variability, especially around the continental boundaries. A clear dipole is visible around the separation location, which hints at shift in the course of the jet. The physical correctness of this shift is discussed in section 3.2 using a more local analysis. The Agulhas return current is an eddy-rich region, and we see an increase in the SFS SST variability in a large swath of this region. The same is also true for the South Atlantic current, where a large number of locations possess $10 - 30\%$ increase in the SST variability. However, a region of decreased SST variability is seen around the Brazil-Malvinas confluence between 30°−60°W and 35°−45°S. The exact reason for this dip is not known, but may be related to the seasonal southward shift of the South Atlantic Current that Kenigson et al. (2022) found when analyzing the effects of this parameterization in a forced-ocean simulation. We also analyzed the ratio of the standard deviations of SFS LHF but found them qualitatively similar and they are therefore not discussed here.

3.2 Correlations

Here we discuss the instantaneous and tendency correlations (as described in section 2.3) for the low-pass fields obtained using spatial filtering with filter sizes between 200−800 km. We compute the correlations for both Control and Stoch simulations and compare them against OBS. We aim to establish physical significance of the parameterized density perturbations by studying their influence on large-scale patterns' correlations and the associated transition length scale at which the THF variability changes from ocean-driven to atmospheric-driven. The transition length scale is computed as the filter width cutoff at which the instantaneous and tendency correlation magnitudes intersect (Bishop et al., 2017). The correlation relationships discussed here are local in nature and belong to the locations marked by a star in Figure 2 in each of the four frontal regions. These locations have two important properties: (i) they possess high SFS SST variability (cf. the SFS SST standard deviation contours in Figure 2), and (ii) the parameterization made a significant change in SFS variability at these locations, e.g., here all locations exhibit more than 15% change in their SFS SST standard deviation.

The GS, Kuroshio, and Agulhas locations show higher instantaneous correlations for Stoch than Control for all filter lengths (Fig. 3, right column); the opposite is true for the tendency correlations. Physically this means that the parameterization is boosting the ocean-intrinsic THF variability and diminishing the fraction of THF that is atmospheric-forced across all scales at these locations. The augmentation of ocean-forced THF variability by the parameterization is consistent with OBS (Fig. 3, left column), as the Control instantaneous correlations are much smaller than OBS for nearly all filter sizes at these mesoscale-eddy-rich locations. Only in Kuroshio, Stoch THF variability goes too strongly ocean-forced compared to OBS beyond 500 km filter width. Modifications in the correlations by the stochastic parameterization are most pronounced near the smallest filter size (200 km), where the Control instantaneous correlations are too low and the tendency correlations are too high compared to OBS – especially for the GS and Kuroshio locations. However, despite the reinforcement, the Stoch instantaneous correlations are generally lower than the corresponding OBS values. A perfect match between Stoch and OBS is nevertheless not expected because the stochastic parameterization used here only accounts for one process (density variations), whereby ocean mesoscales induce variability at larger scales.

The results for the BMC location are different from the other three locations, as it experiences a decrease in the instantaneous correlation and an increase in the tendency correlations across all filter sizes when subjected to the parameterization. The reason behind this is the seasonal southward shift in the Brazil current, and, therefore, the BMC location, as a response to the intense parameterized density correction in this region (Kenigson et al., 2022). Owing to this shift, the THF variability at the BMC location is more atmospheric-

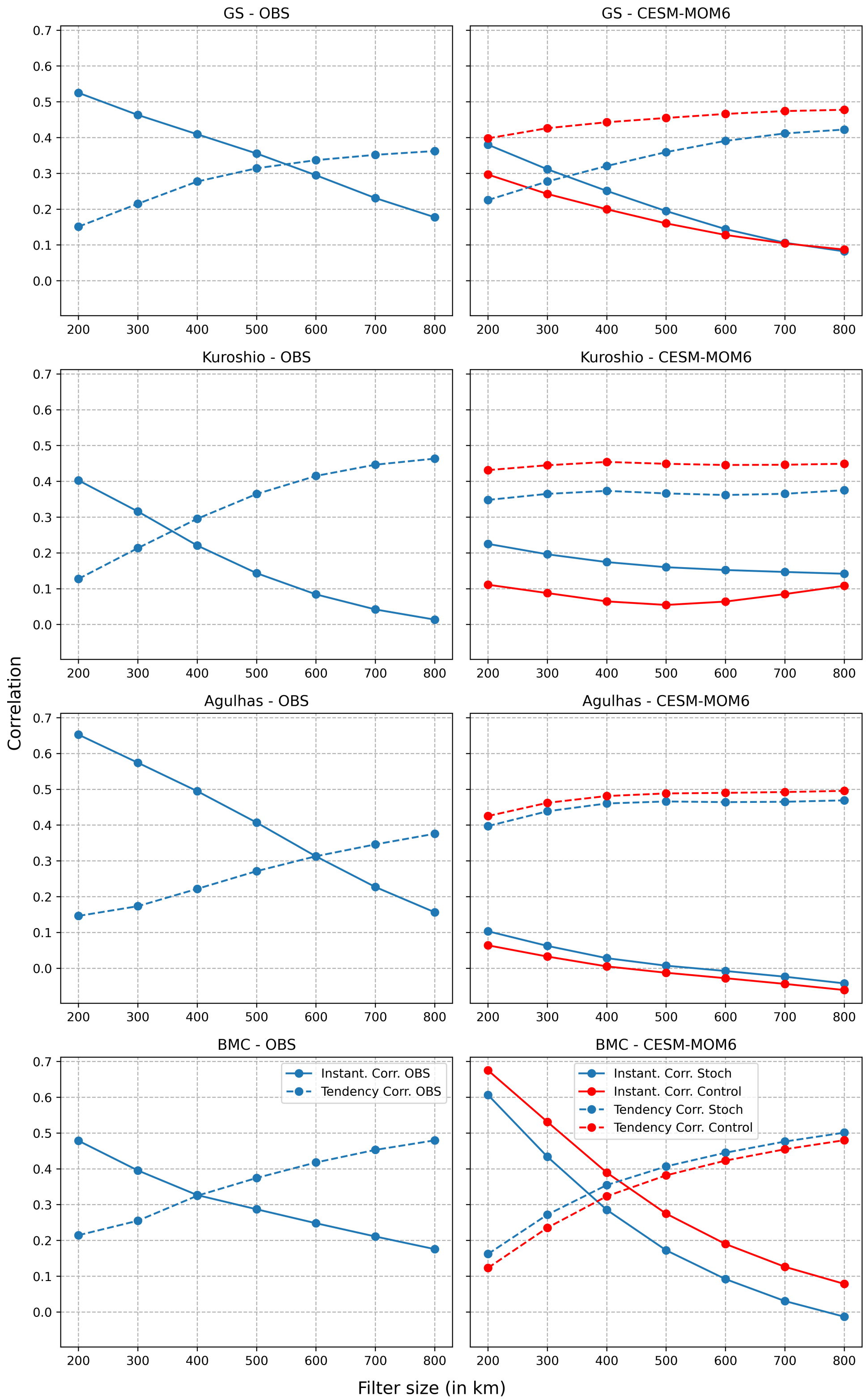

Figure 3. Comparison of local correlations around major WBCs and their scale dependence. Solid lines denote the instantaneous correlations and tendency correlations are depicted in dotted lines. The left column belongs to OBS and the right one corresponds to CESM-MOM6 results. In the right panels, blue/red curves belong to Stoch/Control runs. The rows correspond to the chosen locations marked by stars in Figure 2. The filter length around which the instantaneous and tendency correlation curves intersect is the transition length scale.

driven in the Stoch outputs. This is consistent with OBS for 200−300 km filter sizes; outside this filter limit, Stoch's instantaneous correlations are much smaller than OBS's. Little difference exists between Stoch and Control tendency correlations in this region, and both are close to the OBS magnitudes for all filter sizes.

Finally, we analyze the transition length scale, i.e., the length scale at which LHF variability switches from ocean-driven to atmospheric-driven. The induced stochastic parameterization revises the transition lengths at all chosen locations and pushes them closer to the reference truth – the OBS values. This is clearer in the GS case, where the addition of the stochastic parameterization increases the transition scale from $\approx$ 70 km (not shown) to $\approx$ 350 km, which is closer to but still below the OBS value of $\approx$ 550 km. At the BMC location, Stoch offers a smaller transition scale ($\approx$ 380 km) than Control ($\approx$ 440 km), yet slightly closer to the OBS value ($\approx$ 400 km). At the Kuroshio and Agulhas locations, the Control and Stoch THF outputs are atmospherically driven at the grid scale, and, therefore, the transition length scale is not defined. However, Stoch is less atmospheric-dominated and more ocean-dominated than Control, implying a bigger transition length scale than Control.

4 Conclusions and Discussion

We implemented a physics-based stochastic subgrid-scale (SGS) parameterization for ocean density in a CESM-MOM6 coupled climate model and studied its impact on air-sea turbulent heat flux (THF) variability, primarily latent heat flux (LHF). Past studies have shown that the air-sea flux variability is driven by oceanic-intrinsic variability at ocean mesoscales and by synoptic-scale atmospheric processes at larger scales, e.g., $\mathcal{O}(1000)$ km. But, due to the spatial resolution of non-eddying ocean climate models, the air-sea flux variability due to intrinsic oceanic turbulence is not well represented. Here, we show that a SGS density parameterization successfully restores a significant portion of the missing ocean-intrinsic air-sea THF variability across turbulent, eddy-rich regions, such as western boundary currents and the adjacent re-circulation zones. This study is the first in its kind which shows the revival of intrinsic ocean-driven THF variability in a comprehensive coupled climate model using a systematic physics-based SGS parameterization.

The results presented in this paper are based on a localized study around four WBC regions – Gulf Stream (GS), Kuroshio, Agulhas, and Brazil-Malvinas Confluence (BMC) – and involves subfilter-scale (SFS) fields obtained using a highly scale-selective spatial filter. The parameterization significantly influences SFS SST and LHF variability around the western boundary current regions, as several locations display more than 30% increase in their standard deviation (figure 2). Instantaneous SST-LHF correlations and $\partial\mathrm{SST}/\partial t$ - LHF tendency correlations as a function of the filter scale revealed the impact of the parameterization on large-scale SST-LHF covariability and the associated transition scales. We established that the changes in the SFS SST and LHF variances produced by the parameterization are physically significant as they cascade to larger scales and yield substantial modifications in the mean fields' correlations, which were found consistent with the high-resolution J-OFURO3 observations. Although the high-/low-pass fields used in this paper are obtained using the Taper filtering kernel following Grooms et al. (2021), a Gaussian filtering kernel was also tested. The latter resulted in qualitatively similar results with a slight drop in the instantaneous SST-LHF correlations and an increase in the $\partial\mathrm{SST}/\partial t$ - LHF tendency correlations; therefore, our results are robust to filtering kernels. The comparison of a pre-industrial climate simulation to modern observations is a limitation of this study. Nevertheless, the conclusion that the stochastic parameterization leads to increases in ocean-intrinsic air-sea heat flux variability is not likely to be sensitive to climate changes.

This work has significant potential for further advancements. One possible line of extension is a systematic study of seasonal dependence of the correlations and the transition length scales while focusing on their physical mechanisms. Another possible refinement is to make the whole study more consistent by considering a CESM-MOM6 simulation with a spatial resolution similar to the observations (1/4° here). Presently the observations have more spatial scales resolved and higher variance across scales than the model output. It may also be valuable to develop a physics-based stochastic parameterization for small-scale air-sea flux variability by directly manipulating bulk flux formulas, which possess significant covariability among its constituent variables – all interacting in a nonlinear fashion.

Data Availability Statement

The CESM-MOM6 outputs and the Python analysis scripts used in this work are available in the Zenodo repository: https://doi.org/10.5281/zenodo.7359120. The coupled CESM-MOM6 datasets for other earth system components, e.g., atmosphere, land (not used in this work), are available upon request. The J-OFURO3 observations are available for download from the official J-OFURO project website (https://www.j-ofuro.com/en/dataset/entry-323.html).

Acknowledgments

The authors are grateful to Jessica Kenigson and Alistair Adcroft for helping implement the EOS parameterization inside Gent-McWilliams and the mixed-layer restratification parameterizations in MOM6. NA is also thankful to Gustavo Marques for the help in running CESM-MOM6 coupled simulations. This work of IG and NA was supported by NSF grant OCE 1736708. Computing resources (doi:10.5065/D6RX99HX Computational and Information Systems Laboratory, 2019) were provided by the Climate Simulation Laboratory at NCAR's Computational and Information Systems Laboratory, sponsored by the National Science Foundation and other agencies.

References

Adcroft, A., Anderson, W., Balaji, V., Blanton, C., Bushuk, M., Dufour, C. O., … others (2019). The gfdl global ocean and sea ice model om4. 0: Model description and simulation features. *Journal of Advances in Modeling Earth Systems*, *11*(10), 3167–3211.

Adcroft, A., & Campin, J.-M. (2004). Rescaled height coordinates for accurate representation of free-surface flows in ocean circulation models. *Ocean Modelling*, *7*(3-4), 269–284.

Agarwal, N., Ryzhov, E., Kondrashov, D., & Berloff, P. (2021). Correlation-based flow decomposition and statistical analysis of the eddy forcing. *Journal of Fluid Mechanics*, *924*.

Bishop, S. P., Small, R. J., Bryan, F. O., & Tomas, R. A. (2017). Scale dependence of midlatitude air–sea interaction. *Journal of Climate*, *30*(20), 8207–8221.

Brankart, J.-M. (2013). Impact of uncertainties in the horizontal density gradient upon low resolution global ocean modelling. *Ocean Modelling*, *66*, 64–76.

Computational and Information Systems Laboratory. (2019). *Cheyenne: HPE/SGI ICE XA System (Climate Simulation Laboratory).* doi: 10.5065/D6RX99HX

Czaja, A., Frankignoul, C., Minobe, S., & Vannière, B. (2019). Simulating the midlatitude atmospheric circulation: what might we gain from high-resolution modeling of air-sea interactions? *Current Climate Change reports*, *5*(4), 390–406.

Danabasoglu, G., Lamarque, J.-F., Bacmeister, J., Bailey, D., DuVivier, A., Edwards, J., … others (2020). The community earth system model version 2 (cesm2). *Journal of Advances in Modeling Earth Systems*, *12*(2), e2019MS001916.

Dunstone, N., Smith, D., Scaife, A., Hermanson, L., Eade, R., Robinson, N., … Knight, J. (2016). Skilful predictions of the winter north atlantic oscillation one year ahead. *Nature Geoscience*, *9*(11), 809–814.

Foussard, A., Lapeyre, G., & Plougonven, R. (2019). Storm track response to oceanic eddies in idealized atmospheric simulations. *Journal of Climate*, *32*(2), 445–463.

Fox-Kemper, B., Ferrari, R., & Hallberg, R. (2008). Parameterization of mixed layer eddies. part i: Theory and diagnosis. *Journal of Physical Oceanography*, *38*(6), 1145–1165.

Frankignoul, C., & Hasselmann, K. (1977). Stochastic climate models, part ii application to sea-surface temperature anomalies and thermocline variability. *Tellus*, *29*(4), 289–305.

Frankignoul, C., & Kestenare, E. (2002). The surface heat flux feedback. part i: Estimates from observations in the atlantic and the north pacific. *Climate dynamics*, *19*(8), 633–647.

Gent, P. R., & McWilliams, J. C. (1990). Isopycnal mixing in ocean circulation models. *Journal of Physical Oceanography*, *20*(1), 150–155.

Griffies, S. M., Adcroft, A., & Hallberg, R. W. (2020). A primer on the vertical lagrangian-remap method in ocean models based on finite volume generalized vertical coordinates. *Journal of Advances in Modeling Earth Systems*, *12*(10), e2019MS001954.

Grooms, I., Loose, N., Abernathey, R., Steinberg, J. M., Bachman, S. D., Marques, G., … Yankovsky, E. (2021). Diffusion-based smoothers for spatial filtering of gridded geophysical data. *Journal of Advances in Modeling Earth Systems*, *13*(9), e2021MS002552. Retrieved from `https://agupubs.onlinelibrary.wiley.com/doi/abs/10.1029/2021MS002552` doi: https://doi.org/10.1029/2021MS002552

Hasselmann, K. (1976). Stochastic climate models part i. theory. *tellus*, *28*(6), 473–485.

Hausmann, U., Czaja, A., & Marshall, J. (2017). Mechanisms controlling the sst air-sea heat flux feedback and its dependence on spatial scale. *Climate Dynamics*, *48*(3), 1297–1307.

Hunke, E. C., Lipscomb, W. H., Turner, A. K., Jeffery, N., & Elliott, S. (2010). Cice: the los alamos sea ice model documentation and software user's manual version 4.1 la-cc-06-012. *T-3 Fluid Dynamics Group, Los Alamos National Laboratory*, *675*, 500.

Jansen, M. F., Adcroft, A., Khani, S., & Kong, H. (2019). Toward an energetically consistent, resolution aware parameterization of ocean mesoscale eddies. *Journal of Advances in Modeling Earth Systems*, *11*(8), 2844–2860.

Kenigson, J., Adcroft, A., Bachman, S., Castruccio, F., Grooms, I., Pegion, P., & Stanley, Z. (2022). Parameterizing the impact of unresolved temperature variability on the large-scale density field: 2. modeling. *Journal of Advances in Modeling Earth Systems*, *14*(3), e2021MS002844.

Kuo, Y.-H., Low-Nam, S., & Reed, R. J. (1991). Effects of surface energy fluxes during the early development and rapid intensification stages of seven explosive cyclones in the western atlantic. *Monthly Weather Review*, *119*(2), 457–476.

Large, W. G., McWilliams, J. C., & Doney, S. C. (1994). Oceanic vertical mixing: A review and a model with a nonlocal boundary layer parameterization. *Reviews of geophysics*, *32*(4), 363–403.

Loose, N., Abernathey, R., Grooms, I., Busecke, J., Guillaumin, A., Yankovsky, E., … Martin, P. (2022). Gcm-filters: A python package for diffusion-based spatial filtering of gridded data. *Journal of Open Source Software*, *7*(70), 3947. Retrieved from `https://doi.org/10.21105/joss.03947` doi:

10.21105/joss.03947

Ma, X., Chang, P., Saravanan, R., Montuoro, R., Nakamura, H., Wu, D., … Wu, L. (2017). Importance of resolving kuroshio front and eddy influence in simulating the north pacific storm track. *Journal of Climate*, *30*(5), 1861–1880.

Ma, X., Jing, Z., Chang, P., Liu, X., Montuoro, R., Small, R. J., … others (2016). Western boundary currents regulated by interaction between ocean eddies and the atmosphere. *Nature*, *535*(7613), 533–537.

Marshall, D. P., Maddison, J. R., & Berloff, P. S. (2012). A framework for parameterizing eddy potential vorticity fluxes. *Journal of Physical Oceanography*, *42*(4), 539–557.

Minobe, S., Kuwano-Yoshida, A., Komori, N., Xie, S.-P., & Small, R. J. (2008). Influence of the gulf stream on the troposphere. *Nature*, *452*(7184), 206–209.

Parfitt, R., Czaja, A., Minobe, S., & Kuwano-Yoshida, A. (2016). The atmospheric frontal response to sst perturbations in the gulf stream region. *Geophysical Research Letters*, *43*(5), 2299–2306.

Park, S., Deser, C., & Alexander, M. A. (2005). Estimation of the surface heat flux response to sea surface temperature anomalies over the global oceans. *Journal of climate*, *18*(21), 4582–4599.

Shevchenko, I., & Berloff, P. (2015). Multi-layer quasi-geostrophic ocean dynamics in eddy-resolving regimes. *Ocean Modelling*, *94*, 1–14.

Small, R. J., Bryan, F. O., Bishop, S. P., & Tomas, R. A. (2019). Air–sea turbulent heat fluxes in climate models and observational analyses: What drives their variability? *Journal of Climate*, *32*(8), 2397–2421.

Small, R. J., deSzoeke, S. P., Xie, S. P., O'neill, L., Seo, H., Song, Q., … Minobe, S. (2008). Air–sea interaction over ocean fronts and eddies. *Dynamics of Atmospheres and Oceans*, *45*(3-4), 274–319.

Stanley, Z., Grooms, I., Kleiber, W., Bachman, S., Castruccio, F., & Adcroft, A. (2020). Parameterizing the impact of unresolved temperature variability on the large-scale density field: Part 1. theory. *Journal of Advances in Modeling Earth Systems*, *12*(12), e2020MS002185.

Thompson, L. A., & Kwon, Y.-O. (2010). An enhancement of low-frequency variability in the kuroshio–oyashio extension in ccsm3 owing to ocean model biases. *Journal of climate*, *23*(23), 6221–6233.

Tomita, H., Hihara, T., Kako, S., Kubota, M., & Kutsuwada, K. (2019). An introduction to j-ofuro3, a third-generation japanese ocean flux data set using remote-sensing observations. *Journal of Oceanography*, *75*(2), 171–194.

von Storch, J.-S. (2000). Signatures of air–sea interactions in a coupled atmosphere–ocean gcm. *Journal of Climate*, *13*(19), 3361–3379.

Williams, P. D. (2012). Climatic impacts of stochastic fluctuations in air–sea fluxes. *Geophysical Research Letters*, *39*(10).

Wright, D. G. (1997). An equation of state for use in ocean models: Eckart's formula revisited. *Journal of Atmospheric and Oceanic Technology*, *14*(3), 735–740.

Wu, R., Kirtman, B. P., & Pegion, K. (2006). Local air–sea relationship in observations and model simulations. *Journal of climate*, *19*(19), 4914–4932.

Xie, S.-P. (2004). Satellite observations of cool ocean–atmosphere interaction. *Bulletin of the American Meteorological Society*, *85*(2), 195–208.